Cellular/Molecular

Selective Glycine Receptor α2 Subunit Control of Crossover Inhibition between the On and Off Retinal Pathways

Regina D. Nobles,[1,2] **Chi Zhang,**[1,3] **Ulrike Müller,**[4,5] **Heinrich Betz,**[4] and **Maureen A. McCall**[1,2,3]

Departments of [1]Ophthalmology and Visual Science, [2]Psychological and Brain Sciences, and [3]Anatomical Sciences and Neurobiology, University of Louisville, Louisville, Kentucky 40202, [4]Max Planck Institute for Brain Research, Department of Neurochemistry, 60528 Frankfurt am Main, Germany, and [5]Institute for Pharmacology and Molecular Biotechnology, Department of Bioinformatics and Functional Genomics, University of Heidelberg, 69120 Heidelberg, Germany

In the retina, the receptive fields (RFs) of almost all ganglion cells (GCs) are comprised of an excitatory center and a suppressive surround. The RF center arises from local excitatory bipolar cell (BC) inputs and the surround from lateral inhibitory inputs. Selective antagonists have been used to define the roles of GABA$_A$ and GABA$_C$ receptor-mediated input in RF organization. In contrast, the role of glycine receptor (GlyR) subunit-specific inhibition is less clear because the only antagonist, strychnine, blocks all GlyR subunit combinations. We used mice lacking the GlyRα2 ($Glra2^{-/-}$) and GlyRα3 ($Glra3^{-/-}$) subunits, or both ($Glra2/3^{-/-}$), to explore their roles in GC RF organization. By comparing spontaneous and visually evoked responses of WT with $Glra2^{-/-}$, $Glra3^{-/-}$ and $Glra2/3^{-/-}$ ON- and OFF-center GCs, we found that both GlyRα2 and GlyRα3 modulate local RF interactions. In the On pathway, both receptors enhance the excitatory center response; however, the underlying inhibitory mechanisms differ. GlyRα2 participates in crossover inhibition, whereas GlyRα3 mediates serial inhibition. In the Off pathway, GlyRα2 plays a similar role, again using crossover inhibition and enhancing excitatory responses within the RF center. Comparisons of single and double KOs indicate that GlyRα2 and GlyRα3 inhibition are independent and additive, consistent with the finding that they use different inhibitory circuitry. These findings are the first to define GlyR subunit-specific control of visual function and GlyRα2 subunit-specific control of crossover inhibition in the retina.

Introduction

The spatiotemporal interplay of excitatory and inhibitory inputs underlies both the receptive field (RF) organization and the sustained/transient nature of retinal ganglion cell (GC) responses. Together they provide the basis for their ability to extract information from the visual scene. Both GABA and glycine inhibition are used to modulate different aspects of GC responses and RF organization (Caldwell and Daw, 1978; Flores-Herr et al., 2001; O'Brien et al., 2003; Chen et al., 2010, 2011). Ionotropic GABA receptors (GABARs) and glycine receptors (GlyRs) are agonist-gated chloride channels that provide the majority of this modulation. Both GABARs and GlyRs are composed of subunit combinations that create inputs with diverse kinetics, agonist affinities, and desensitization characteristics (Bormann, 2000; Webb and Lynch, 2007). The availability of selective antagonists have defined the roles of GABA$_A$R- and GABA$_C$R-mediated in-

hibition within the retinal circuit (for review, see Eggers and Lukasiewicz, 2011). GABARs are the receptor targets of amacrine cells (ACs), whose broad lateral processes ramify within one of the two sublamina (On or Off) of the inner plexiform layer (IPL) (MacNeil et al., 1999). GABAergic ACs target GABA$_A$Rs and GABA$_C$Rs in reciprocal inhibitory circuits to modulate RF center excitation (Eggers et al., 2007; Grimes et al., 2010). Similarly, they target GABA$_A$Rs to modulate serial inhibition (Eggers and Lukasiewicz, 2010), to amplify and refine the RF surround (Cook and McReynolds, 1998; Roska et al., 2000; O'Brien et al., 2003).

GlyRs are the targets of glycinergic ACs whose narrow lateral processes ramify across the On and Off IPL sublaminae (MacNeil and Masland, 1998; Menger et al., 1998). GlyR inputs use crossover or feedforward inhibition to modulate GC RF center excitation (Wässle et al., 1986; Stone and Pinto, 1992; MacNeil and Masland, 1998; O'Brien et al., 2003; Chen et al., 2010; Russell and Werblin, 2010). The chloride channels formed by synaptic GlyRs are heteromeric and contain two α and three β subunits (Grudzinska et al., 2005). GlyRs containing different α subunit isoforms (α1, α2, α3, or α4) display distinct IPL and neuronal subtype localization. Specifically, GlyRα1 is the predominant and perhaps only α subunit expressed by Off cone and rod bipolar cells (BCs) (Sassoè-Pognetto et al., 1994; Enz and Bormann, 1995; Cui et al., 2003; Ivanova et al., 2006). Although GlyRα1 modulates a significant inhibitory input to A-type murine GCs, GlyRα2, GlyRα3, and GlyRα4 also contribute to sIPSCs in these cells (Majumdar et al., 2007). Given the differences in localization, as well as current decay properties (for review, see Wässle et al., 2009) it

is likely that GlyR subunits like GABA$_A$R and GABA$_C$Rs participate in specific inhibitory mechanisms and circuits that control retinal function. Also like GABA$_A$Rs, a lack of subunit-specific antagonists has prevented the definition of individual GlyR subunit-specific control of visual function.

Using a molecular genetic approach and GlyRα2 and α3 subunit knock-out (KO) mice, we defined subunit-specific inhibition in GC RF center responses. Our results define for the first time that (1) GlyRα2 and GlyRα3 inhibition enhance GC RF excitatory center responses, (2) GlyRα2 modulates crossover inhibition in both the On and Off pathways, and (3) GlyRα2 crossover and GlyRα3 serial inhibition are additive and independent in the On pathway.

Materials and Methods

Animals. We used male and female C57BL/6J wild-type (WT) mice (Jackson Laboratory) and two KO mouse lines that lacked GlyRα2 (*Glra2*$^{-/-}$) (Young-Pearse et al., 2006) or GlyRα3 (*Glra3*$^{-/-}$) (Harvey et al., 2004) subunit expression. The *Glra2/3*$^{-/-}$ double KO mice were generated by crossing and backcrossing the single KO lines. Genotypes were verified by PCR using primers and cycling conditions published previously (Harvey et al., 2004; Young-Pearse et al., 2006). All mice were maintained at the University of Louisville on a 12 h light/dark schedule. All experimental procedures were conducted in accordance with regulations described for the ethical care and treatment of animals in the Society for Neuroscience Policies on the Use of Animals in Neuroscience Research and in compliance with a protocol approved by the University of Louisville Institutional Animal Care and Use Committee.

Surgical preparation for electrophysiology recordings from optic nerve fibers. All surgical procedures were performed at light-adapted levels and have been published previously (Sagdullaev and McCall, 2005). Briefly, anesthesia was induced with an intraperitoneal injection of a Ringer's solution containing ketamine and xylazine. In WT mice, the induction dose was 127:12 mg/kg. In *Glra2*$^{-/-}$ and *Glra2/3*$^{-/-}$ mice, an increase of 12.5% was required to induce a surgical plane of anesthesia. Anesthesia was maintained throughout the experiments with supplemental subcutaneous injections (50% of initial concentration) administered every 45 min. The head was secured in a stereotaxic frame (David Kopf Instruments) with ear cups and a bite bar. Body temperature was maintained at 37°C with a feedback-controlled heating pad (TC-1000; CWE). Topical Mydfrin (phenylephrine hydrochloride ophthalmic solution, 2.5%) and Mydriacyl (tropicamide ophthalmic solution, 1%; Alcon Labs) were applied to dilate the pupils and paralyze accommodation. To prevent drying of the corneas, clear zero-powered lenses (Sagdullaev et al., 2004) moistened with artificial tears (Akwa Tears; Akorn) were placed over the eyes. A craniotomy was performed anterior to the Bregma suture and the overlying cortex was removed using suction to expose the optic nerve.

In vivo *electrophysiology recordings from optic nerve fibers.* Action potentials were recorded extracellularly from single optic nerve axons using sharpened tungsten electrodes (A-M Systems) with a final impedance between 30–100 MΩ. A reference electrode was inserted subcutaneously. Action potentials from single GC axons were isolated, amplified (X3−Cell; FHC), digitized at 15 kHz (Power1401; Cambridge Electronic Design), and stored for offline analysis. The isolated spikes were simultaneously displayed on an oscilloscope (60 MHz; Tektronix) and computer monitor (Spike2; Cambridge Electronic Design) and played over an audio monitor (AM7; Grass Instruments) to obtain direct feedback of the cell's response. Responses were analyzed offline using Spike2 software version 4.24 (Cambridge Electronic Design). Spikes were accumulated within a 50 ms bin width and displayed as poststimulus time histograms (PSTHs). Each average PSTH was smoothed by fitting it with a raised cosine function with a 50 ms smoothing interval to minimize alteration of the peak firing rate and maximize signal-to-noise ratio (Sagdullaev and McCall, 2005).

Quantitative characterization of GC visual response properties. The spatial extent and RF center sign of each GC was mapped using a handheld light source on a removable screen that covered a CRT display monitor
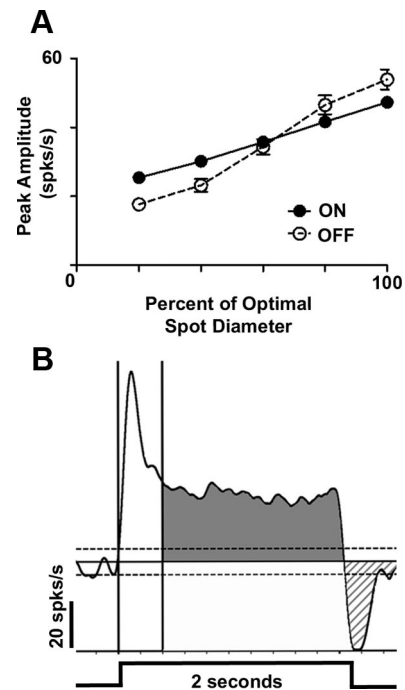

Figure 1. Representative area response function and PSTH response quantification during receptive field center stimulation. *A*, Representative ARFs for WT ON (filled circles) and OFF (open circles) GCs. These ARFs plot the peak amplitude (defined as: peak − spontaneous firing rate) of the GC excitatory response as a function of the spot outer diameter up to the maximum response, which represents the spot diameter that matches the receptive field center size. This spot diameter is referred to as the optimal spot. *B*, A representative PSTH from a sustained ON GC to an optimal spot presented for a duration of 2 s (stimulus profile at bottom of PSTH). We defined the excitatory response when the firing rate crosses above +3 SEM of the mean spontaneous activity ($\bar{x}$SA, top dotted line) until the response returns to the $\bar{x}$SA (solid line). The vertical cursors define the transient response component (0 – 0.4 s). The shaded region represents the maintained response component (0.4 –2.0 s). The hatched region (below $\bar{x}$SA) represents response suppression at stimulus offset when the spiking rate drops below −3 SEM $\bar{x}$SA (bottom dotted line) until the response returns to the $\bar{x}$SA.

(Eizo E120 FlexScan FXC7). The screen was located 20–25 cm from the anterior nodal point of the eye. All stimulus and RF dimensions are corrected for monitor distance and are presented in the text in degrees of visual angle.

Receptive field center analysis. Computer generated stimuli (Vision-Works; Vision Research Graphics) were presented on a CRT monitor with a mean luminance of 20 cd/m^2. Stimulus luminance increased to 100 cd/m^2 for ON GCs and decreased to 3 cd/m^2 (67% contrast) for OFF GCs. Stationary spots of increasing outer diameter (eight steps from 4.6 to 52.7°) were centered on the RF and presented in random order with randomly interleaved blank trials. Spots were presented for 2 s with a 5 s interstimulus interval. The mean spontaneous activity ($\bar{x}$SA) was measured from "blank" trials, where the monitor luminance was 20 cd/m^2. ±3 SEM of the SA was used as a criterion to define thresholds for excitatory and suppressive responses.

Both peak and maintained firing rate were plotted as a function of spot diameter and formed an area response function (ARF) (Fig. 1*A*). We used the ascending limb of the ARF and its slope to evaluate spatial summation within the RF center, which results from the recruitment of excitatory BC input. The stimulus that elicited the maximum excitatory response defined the RF center diameter and is referred to as the optimal spot.

Excitatory response characteristics. We quantitatively characterized several aspects of the excitatory response from the average PSTH evoked by the optimal spot (Fig. 1*B*). Onset latency was defined as the time from stimulus onset until the time when the response rose to 3 SEM above $\bar{x}$SA. Excitatory response duration was defined as the duration from response onset to offset, when the response decreased below $\bar{x}$SA. The total excit-
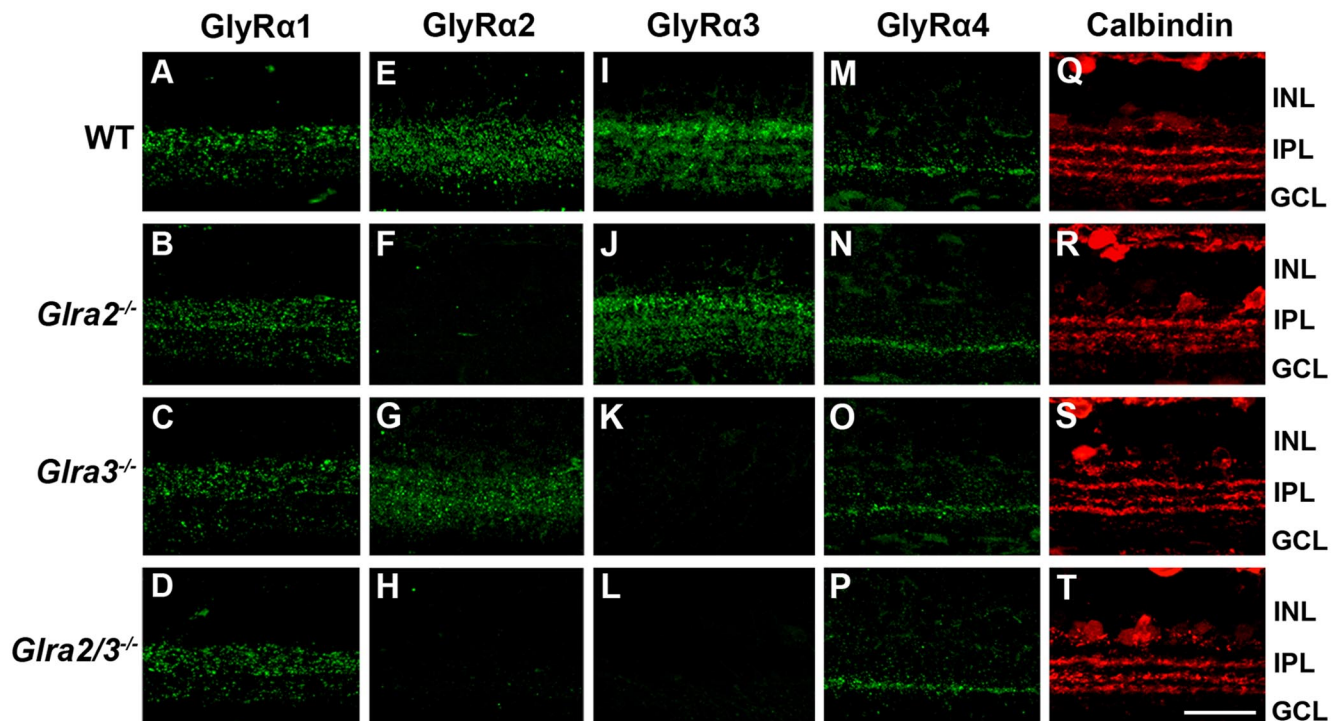
Figure 2. GlyRα subunit expression across WT, $Glra2^{-/-}$, $Glra3^{-/-}$ and $Glra2/3^{-/-}$ retinas. **A–T**, Representative confocal images of transverse retinal sections (25 μm) reacted with one of four GlyRα subunit-specific antibodies. INL, Inner nuclear layer; IPL, inner plexiform layer; GCL, ganglion cell layer. Scale bar, 20 μm. GlyRα1-immunoreactive puncta are prominent in the outer strata of the IPL across all genotypes (**A–D**). Representative confocal images of GlyRα2-immunoreactive puncta are diffuse across all IPL strata in WT and $Glra3^{-/-}$ retinas (**E, G**) and are absent in $Glra2^{-/-}$ and $Glra2/3^{-/-}$ retina (**F, H**). GlyRα3-immunoreactive puncta label four bands in the IPL of WT and $Glra2^{-/-}$ retinas (**I, J**) and are absent in the $Glra3^{-/-}$ and $Glra2/3^{-/-}$ retina (**K, L**). GlyRα4-immunoreactive puncta are localized to a distinct band within the IPL in all genotypes (**M–P**). Retinas of all genotypes were reacted with an antibody to calbindin (red) and illustrate that IPL sublamination patterns are similar across genotype (**Q–T**).

atory response was defined as the area that remained 3 SEM above $\bar{x}$SA. In WT GCs, the total excitatory response consisted of two components, a transient peak component (Fig. 1, white region), which then decayed to 37% of peak (or $1/e$) within 0.4 s and a maintained component whose duration varied (>0.4 to ≤2.0 s; Fig. 1, gray region). Sustained cells were defined as those whose excitatory response remained 3 SEM above mean spontaneous level for the entire duration of stimulus presentation (2 s). Transient cells had excitatory responses that returned to the mean spontaneous level at ≤1.7 s. We found no ganglion cells whose response durations were between >1.7 and <2.0 s.

Suppressive response characteristics. Using the same average PSTH, we quantified several aspects of response suppression that occurred at stimulus offset (Fig. 1 B, hatched region). Onset latency of suppression was defined as the time from stimulus offset until the time when the response decreased below $\bar{x}$SA. The duration of response suppression was defined as the duration from onset latency of suppression until the response rose to $\bar{x}$SA. The total magnitude of suppression was defined as the area when the response remained below $\bar{x}$SA.

Immunohistochemistry. We examined the morphology of both single- and double KO retinas using fluorescence immunohistochemistry (Gregg et al., 2007). Retinas were removed from the eyecup, fixed for 15–20 min in 4% paraformaldehyde in 0.1 M phosphate buffer (PB), pH 7.4, cryoprotected through a graded series of sucrose (Barthel and Raymond,1990), and embedded in OCT:20% sucrose (2:1) (Sakura Finetek). Retinas from all four genotypes were stacked together in the same mold and frozen in OCT:20% sucrose (2:1). Twenty-five micron transverse sections were cut through all four retinas on a CM 1850 cryostat (Leica) and mounted on microscope slides (Superfrost/Plus; Fischer Scientific). This ensured that each section was reacted under the same experimental protocol and was reacted with the exact same antibody concentration. Slides were brought to room temperature (RT), incubated in blocking solution (10% normal goat serum, 0.5% Triton X-100 in PBS) for 60 min, and incubated with primary antibodies (diluted in blocking solu-

tion) at RT overnight. A mouse monoclonal antibody to GlyRα1 (1:100; Synaptic Systems), goat polyclonal antibody to GlyRα2 and GlyRα3 (both1:50; Santa Cruz Biotechnology), and rabbit polyclonal antibody to GlyRα4 (1:100; Millipore Bioscience Research Reagents) labeled individual GlyRα subunits in WT and single and double KO retinas. A rabbit polyclonal antibody to calbindin (D-28k) (1:1000; Swant) labeled the sublamination pattern of the IPL. Sections were washed in PB and incubated in the secondary antibodies goat anti-mouse, donkey anti-goat, and goat anti-rabbit Alexa 488 in blocking solution for 90 min. Sections were coverslipped with Immu-Mount (Thermo Scientific), and images were taken on an Olympus BX51WI confocal microscope equipped with a Hamamatsu CCD EM digital camera using a 40× PLAPO WLSM objective and FluoView version 5.0 software (Olympus).

Isolation of RNA and reverse transcription. Both retinas were removed from WT and $Glra3^{-/-}$ mice and pooled. Total RNA was extracted from each sample using TRI Reagent (1.0 ml per two retinas) and purified using RiboPure Kit (Ambion). The quantity and quality of the RNA was determined using a NanoDrop 2000 spectrophotometer (Thermo Fisher Scientific). First-strand cDNA synthesis was performed by a reaction of 350 ng of total RNA from each sample using the SuperScript III Reverse Transcriptase (Invitrogen).

Real-time PCR. Real-time PCR was performed on a total of 20 μl of cDNA in reaction mix in 96-well plates using 7900HT Fast Real-Time PCR System (Applied Biosystems). Each 20 μl reaction mixture included 1 μl cDNA, 2 μl TaqMan Fast Universal PCR Master Mix, and 0.5 μl 20× TaqMan assay containing either GlyRα2 or 18s RNA primer sets (GlyRα2, Mm00806742_m1; 18s, Mm03928990_g1; Applied Biosystems). For each cDNA sample, three to four PCR replicates were performed using each primer set. The PCR parameters were: incubation at 50°C for 2 min, denaturation at 95°C for 10 min, and 40 cycles of 95°C for 15 s and 60°C for 1 min. ΔC_T of GlyRα2 in each cDNA sample was normalized to the rRNA 18s as an endogenous control as follows: $\Delta C_T = C_{T,\ GlyR\alpha2} - C_{T,\ 18s}$. Here, C_T is the cycle threshold. The ΔC_T ratio was
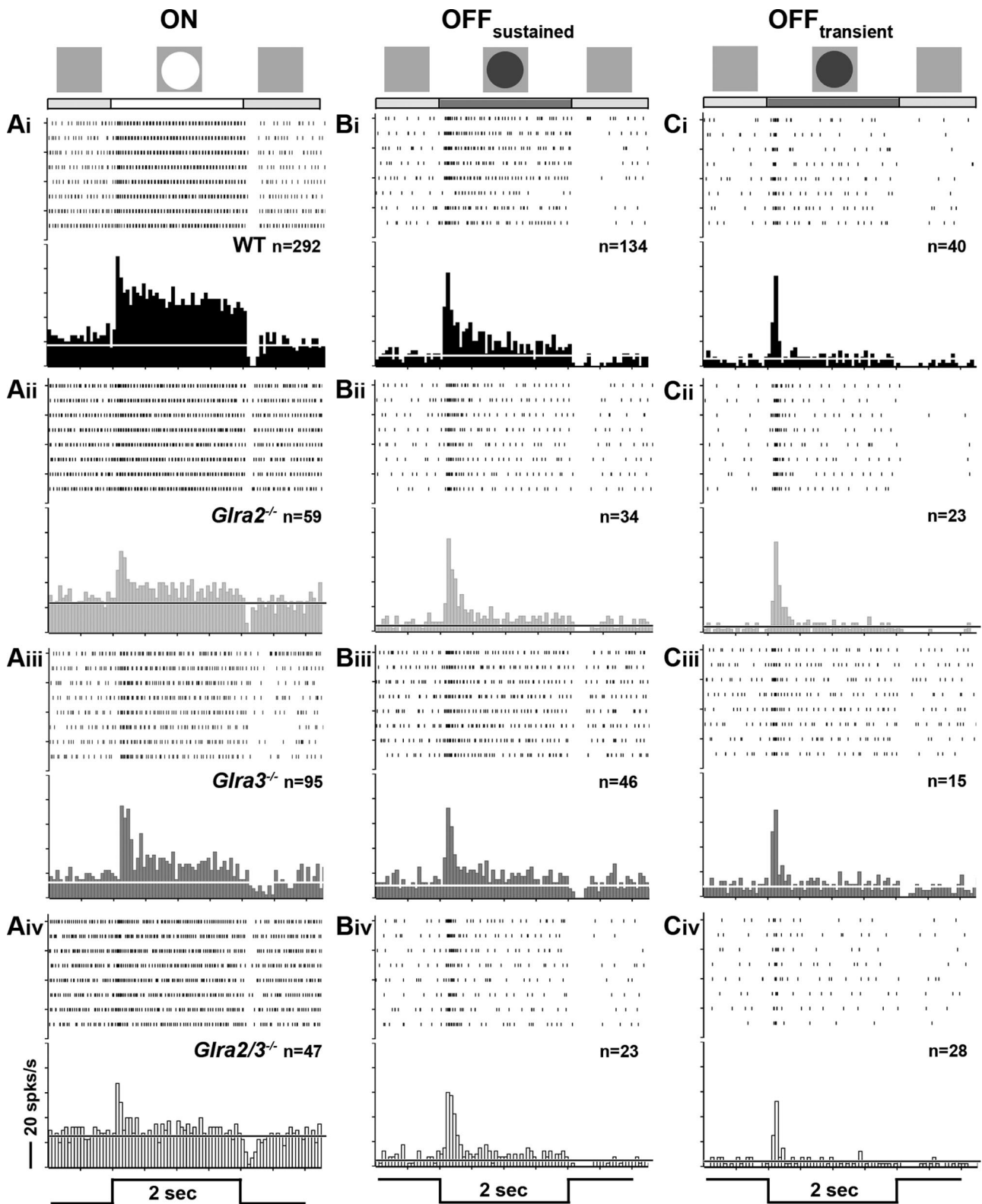
Figure 3. Receptive field center excitatory responses of ON, OFF$_{sustained}$, and OFF$_{transient}$ GCs across genotype. Average PSTHs for ON and OFF GCs evoked by their optimal spot are shown along with the eight individual responses in raster plots (above). The luminance profile of the stimulus (2 s duration) is shown at the bottom of each column. For ON GCs, a bright spot (100 cd/m^2) was presented, and for OFF GCs, a dark spot (3 cd/m^2) was presented on a screen whose average luminance was 20 cd/m^2. Scale bar, 20 spikes per second. **Ai–Aiv**, ON GCs of all genotypes increase spiking at the onset of a bright spot and their excitatory response remains above the $\bar{x}$SA (solid line) for the entire duration of the stimulus. **Bi–Civ**, OFF GCs increase spiking at the onset of dark spot centered on their RFs and can be divided by the duration of their response compared to the stimulus. **Bi–Biv**, OFF$_{sustained}$ GCs respond for the entire duration of the stimulus presentation. **Ci–Civ**, OFF$_{transient}$ GC responses decline to the $\bar{x}$SA before stimulus offset (≤1.70 s).
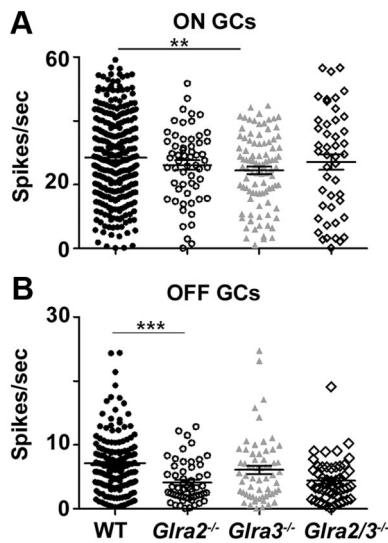
Figure 4. GlyRα3 expression selectively governs ON and GlyRα2 expression governs OFF GC spontaneous activity. *A*, ON GCs. Spontaneous activity is significantly lower in $Glra3^{-/-}$ ON GCs (gray triangles; $n = 94$) compared to WT GCs (filled circles; $n = 291$), but is similar between WT and $Glra2^{-/-}$ ON GCs (open circles; $n = 58$). The spontaneous activity levels do not differ between double KOs (open diamonds; $n = 46$) and single KOs. *B*, OFF GCs. Spontaneous activity is significantly lower in $Glra2^{-/-}$ OFF GCs (open circles; $n = 57$) compared to WT GCs (filled circles; $n = 171$), but similar between WT and $Glra3^{-/-}$ OFF GCs (gray triangles; $n = 61$). The spontaneous activity levels in double KO OFF GCs (open diamonds; $n = 47$) are similar to those in $Glra2^{-/-}$ OFF GCs and single KOs. **$p < 0.01$; ***$p < 0.001$.
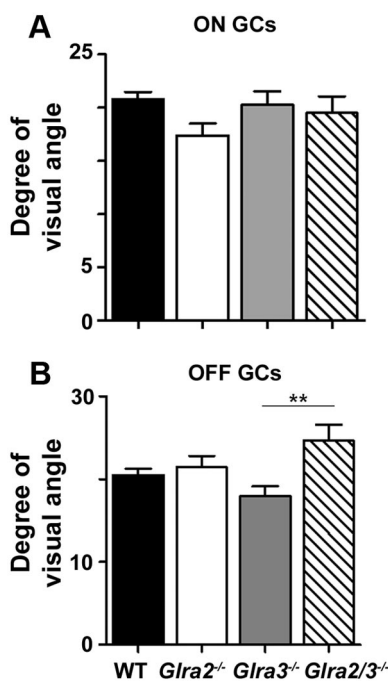

Figure 5. Receptive field center diameter is not affected by the absence of either GlyRα2 or GlyRα3 expression. *A*, ON GCs. The RF center diameters of both single KO ON GCs ($Glra2^{-/-}$, open bar, $n = 59$; $Glra3^{-/-}$, gray bar, $n = 95$) are similar to those of WT (black bar; $n = 292$). The RF center diameters of double KO ON GCs (hatched bar; $n = 47$) were similar to those of both single KO ON GCs. *B*, OFF GCs. The RF center diameters of both single KO OFF GCs ($Glra2^{-/-}$, open bar, $n = 57$; $Glra3^{-/-}$, gray bar, $n = 61$) are similar to those of WT (black bar; $n = 174$). The RF center diameters of double KO OFF GCs (hatched bar; $n = 51$) are similar to those of $Glra2^{-/-}$ OFF GCs, but are significantly larger than those of $Glra3^{-/-}$ OFF GCs. **$p < 0.01$.

Table 1. Receptive field center diameter (degree of visual angle)

GC class	WT			$Glra2^{-/-}$			$Glra3^{-/-}$			$Glra2/3^{-/-}$		
	$\bar{x}$	$\pm$SE	n	$\bar{x}$	$\pm$SE	n	$\bar{x}$	$\pm$SE	n	$\bar{x}$	$\pm$SE	n
ON	20.8	0.7	292	17.4	1.1	59	20.3	1.2	95	19.5	1.6	47
OFF	20.5	0.7	174	21.4	1.4	57	18.0	1.2	61	24.7	1.9	51

The spot outer diameter that elicited the maximum spiking response for ON and OFF GCs is an estimate of the RF center diameter for each genotype. The mean RF diameter ($\bar{x}$), $\pm$SE, and total number (n) of cells are presented for each genotype. RF dimensions are corrected for monitor distance and are presented in degrees of visual angle.

obtained by dividing each ΔC_T by the lowest ΔC_T from the results. The ΔC_T ratios of WT and $Glra3^{-/-}$ mice were compared using a nonparametric t test to examine differences in transcriptional level of GlyRα2.

Statistical analyses. Statistical analyses were performed using Graph-Pad Prism5 software version 5.04 for Windows. Distributions of each response component were tested for normality using the D'Agostino–Pearson omnibus test. The distributions of our quantitative responses across GC types and mouse strains were not normal. As a consequence, wherever possible, we used nonparametric statistical analyses to test for differences. We compared each single KOs to WT and double KOs to each single KO using an unpaired t test with Welch's correction (t test with Welch's). Because our sample size across spot diameter satisfies the central limit theorem, we used a two-way ANOVA to compare responses across spot diameter between genotypes. A linear regression analysis was used to compare changes in the slope of the RF center summation between genotypes. We used a χ^2 analysis to determine any differences in the distributions of transient versus sustained OFF GCs between genotypes. Data in graphs are represented as mean $\pm$ SEM.

Results

Normal inner retinal morphology is retained in the absence of GlyRα2, GlyRα3, or both receptor subunits

In the $Glra3^{-/-}$ mice used in these studies, the absence of GlyRα3 retinal expression has been demonstrated previously (Harvey et al., 2004). In the $Glra2^{-/-}$ mice used here, the absence of retinal expression was verified at the transcription level at P0 (Young-Pearse et al., 2006). We used immunostaining with subunit-specific antibodies to confirm the absence of GlyRα2 and GlyRα3 expression in adult $Glra2^{-/-}$ (Fig. 2, second row), $Glra3^{-/-}$ (third row) and $Glra2/3^{-/-}$ (fourth row) retina sections compared to WT (Fig. 2, first row). Each single KO lacked the characteristic immunoreactivity of its deleted GlyRα subunit, and the double KOs exhibited neither GlyRα2 nor GlyRα3 staining. In both the single and the double KO retinas, the expression patterns of the GlyRα1 and GlyRα4 subunits did not differ from WT (Fig. 2, first and fourth columns). Because GlyRα subunits are expressed primarily in the IPL, we examined and compared the calbindin sublamination pattern in the IPL across WT and single and double KO retinas. Retinas from all four genotypes showed three clear calbindin-immunoreactive bands (Fig. 2, fifth column). Thus, the gross morphology of the inner retina appears intact regardless of the absence of GlyRα2, GlyRα3, or both subunit expression. The GlyRα3 antibody labels four discrete bands in the IPL (Haverkamp et al., 2003), and although moderate upregulation of GlyRα2 expression has been reported across the IPL in the absence of GlyRα3 (Heinze et al., 2007), this difference was not evident in our immunohistochemical analysis.

GlyRα2 transcription levels are not altered in $Glra3^{-/-}$ mice

We used real time PCR to examine the expression of the $Glra2$ gene in WT retina and to determine whether it is upregulated in $Glra3^{-/-}$ retina. Our results show that the level of GlyRα2 mRNA in WT ($n = 9$) and $Glra3^{-/-}$ ($n = 8$) retinas (ΔC_T ratio) was similar (WT, 1.029 ± 0.01; $Glra3^{-/-}$, 1.046 ± 0.016; $p = 0.13$). The electrophysiological data presented below are consistent
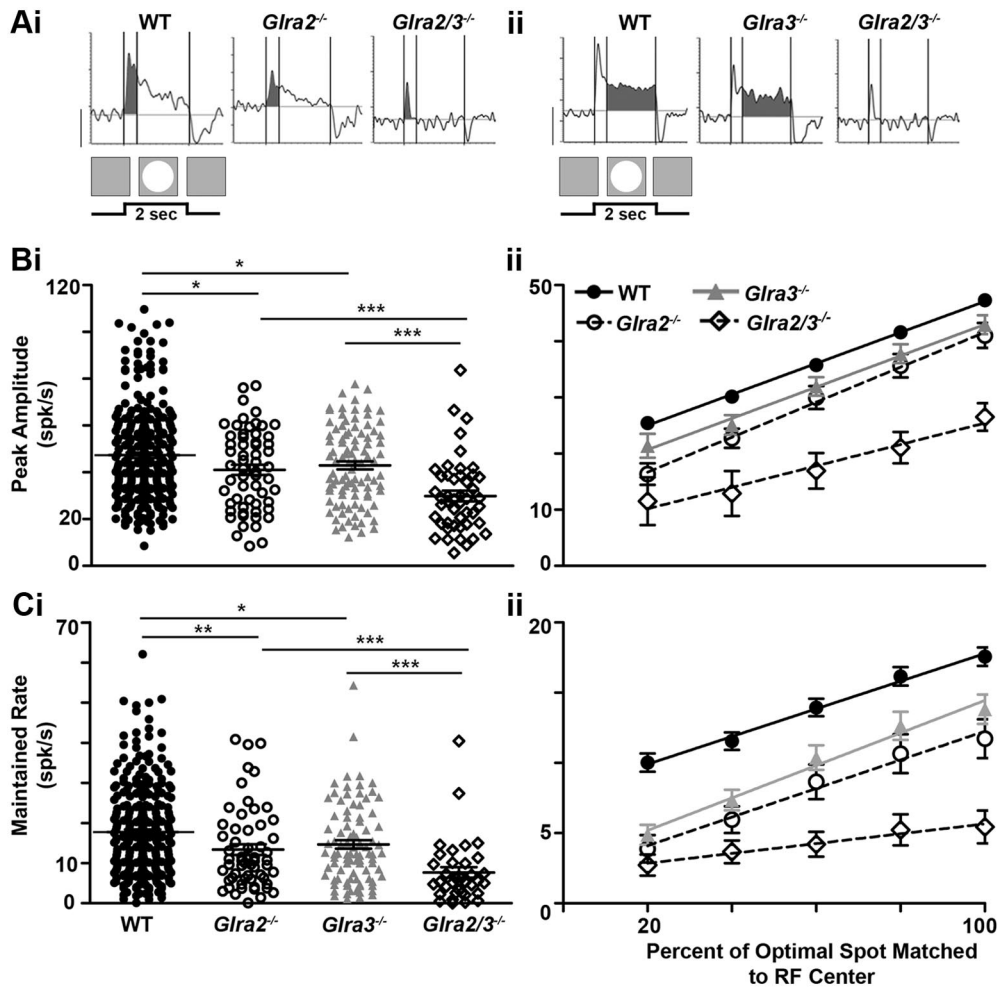
Figure 6. Both GlyRα2- and GlyRα3-mediated inhibition enhances the receptive field center responses of ON GCs. *Ai, Aii*, Representative PSTHs of WT and single- and double KO ON GC RF responses. Shaded regions represent the transient (0 – 0.4 s) response component (*Ai*) and the maintained response component (0.4 –2 s; *Aii*). The stimulus (a bright spot) and its duration profile are shown below the response. *Bi*, The scatter plot shows the distribution of the peak amplitude responses across genotype and illustrates the differences across genotype. The peak amplitudes of both *Glra2*$^{-/-}$ (open circles; $n = 59$) and *Glra3*$^{-/-}$ ON GCs (gray triangles; $n = 95$) are lower than that of WT (closed circles; $n = 292$). The peak amplitude of *Glra2/3*$^{-/-}$ ON GCs (open diamonds; $n = 47$) is lower than the peak amplitude for either single KO. *Bii*, The mean ARFs for each genotype. RF diameter is normalized so that the optimal diameter is plotted at 100%. The slope represents the rate of change in peak amplitude during RF center summation and is similar between WT and single KOs ($p = 0.07$) but differs between single and double KOs ($p < 0.001$). All curves were analyzed using a linear regression and the goodness of fit for all genotypes; $R^2 = 0.99$. *Ci*, The scatter plot shows the distribution of maintained firing rates across genotype and the differences across genotype. The maintained firing rates are lower in *Glra2*$^{-/-}$ (open circles; $n = 57$) and *Glra3*$^{-/-}$ (gray triangles; $n = 90$) compared to WT (closed circles; $n = 289$) and lower in *Glra2/3*$^{-/-}$ (open diamonds; $n = 34$) compared to single KO ON GCs. *Cii*, The mean ARFs for each genotype. RF diameter is normalized so that the optimal diameter is plotted at 100%. The slope represents the rate of change in maintained firing rate during RF center summation and is similar between WT and single KOs ($p = 0.30$) but differs between single and double KOs ($p < 0.0001$). All curves were analyzed using a linear regression and the goodness of fit for all genotypes; $R^2 = 0.98$. Scale bar, 20 spikes per second. *$p < 0.05$; **$p < 0.01$; ***$p < 0.001$.

with this result and suggest that there is no upregulation of GlyRα2 in the absence of GlyRα3.

GlyR subunit-specific inhibition enhances ON and OFF GC spontaneous activity but does not alter receptive field center size

Because little is known about the role of GlyR subunits in GC spontaneous or visually evoked responses, we examined and compared the responses of GCs using spot stimuli of varying diameter to probe their RF center response. We divided GCs into those with ON-center (ON) or OFF-center (OFF) RFs and their responses into excitatory and suppressive phases (Fig. 1*B*). Representative responses of each GC class recorded from all four genotypes are shown in the average PSTHs of Figure 3. Raster plots above each PSTH indicate their spiking responses to individual stimulus presentations. Among our 292 WT ON GCs, we found only 10 cells with transient responses. We divided the

excitatory responses of OFF GCs into transient and maintained components relative to the presence of the stimulus. For each GC response characteristic, we compared WT ON or OFF GCs (Fig. 3*Ai,Bi,Ci*) to GCs from each single KO (Fig. 3*Aii–Ciii*). This allowed us to determine whether one or both subunits modulated the response. We used comparisons of GC responses between single (Fig. 3*Aii–Ciii*) and double KOs (Fig. 3*Aiv–Civ*) to evaluate whether GlyRα2 and GlyRα3 inhibition were independent. Finally, we compared changes in excitatory and suppressive responses in an attempt to determine the synaptic circuit(s) that could account for the changes observed.

The SA of OFF GCs was significantly lower than ON GCs in WT as well as all knock-outs. The SA of *Glra3*$^{-/-}$ ON GCs was significantly lower than that of WT ON GCs (Fig. 4*A*; 24.5 ± 1.2 spikes/s, $n = 94$ vs 28.5 ± 0.8 spikes/s, $n = 291$; $p = 0.005$). The SA of *Glra2*$^{-/-}$ OFF GCs was significantly lower than that of WT

OFF GCs (Fig. 4*B*; 4.1 ± 0.4 spikes/s, $n = 57$ vs 6.8 ± 0.3 spikes/s, $n = 174$; $p < 0.001$). The SA of $Glra2/3^{-/-}$ ON (27.1 ± 2.5 spikes/s; $n = 46$) and OFF GCs (4.7 ± 0.5 spikes/s; $n = 47$) was similar to that of single KO ON ($Glra2^{-/-}$, $p = 0.70$; $Glra3^{-/-}$, $p = 0.30$) and OFF GCs ($Glra2^{-/-}$, $p = 0.47$; $Glra3^{-/-}$, $p = 0.08$) (Fig. 4*A*,*B*). Our results indicate that GlyRα3 and GlyRα2 subunits provide pathway-specific tonic inhibition. GlyRα3 acts within the On pathway, whereas GlyRα2 acts within the Off pathway. Each serves to enhance the tonic spontaneous firing rate of GCs in the WT retina. In light of this finding in the subsequent analyses, SA was subtracted from evoked GC responses in all genotypes.

The RF center diameters of $Glra2^{-/-}$ and $Glra3^{-/-}$ ON (Fig. 5*A*) and OFF (Fig. 5*B*) GCs were similar to those of WT GCs (Table 1; ON, $p = 0.11$, $p = 0.51$; OFF, $p = 0.56$, $p = 0.08$, respectively). The RF diameters of ON single and double KO GCs also were similar ($p = 0.50$ and $p = 0.95$, respectively). The mean RF diameters of double KO OFF GCs, while similar to $Glra2^{-/-}$ ($p = 0.44$), were significantly larger than $Glra3^{-/-}$ ($p = 0.005$). Our results are primarily consistent with previous studies that GlyR modulation does not contribute significantly to RF center spatial tuning (O'Brien et al., 2003; Manookin et al., 2008; van Wyk et al., 2009; Chen et al., 2010). The difference that we observe in the RF diameters of the double KO OFF GCs could be confounded with their generally low response amplitudes and more transient responses, which could lead to the need for larger spots to obtain responses significantly above SA.

WT ON GCs receptive field center excitation is enhanced by both GlyRα2 and GlyRα3 inputs
The onset of a stationary bright spot whose dimensions are within or match the RF center evokes an excitatory response in WT ON GCs. In the overwhelming majority of WT ON GCs in our sample (282 of 292) this excitatory response has an initial transient peak within 0.40 s of stimulus onset (Fig. 6*Ai*, left) followed by a maintained excitation that is temporally matched to the stimulus (2 s) (Fig. 6*Aii*, left). The remaining 10 WT ON GCs had only a transient peak.

The transient peaks of both $Glra2^{-/-}$ (41.0 ± 2.2 spikes/s; $n = 59$) and $Glra3^{-/-}$ ON GCs (43.0 ± 1.7 spikes/s; $n = 95$) were significantly lower than those of WT ON GCs (Fig. 6*Bi*; 47.3 ± 1.2 spikes/s; $n = 292$; $p = 0.02$ and $p = 0.04$, respectively). The maintained firing rates of both $Glra2^{-/-}$ (13.4 ± 1.3 spikes/s; $n = 57$) and $Glra3^{-/-}$ ON GCs (14.7 ± 1.0 spikes/s; $n = 90$) also were significantly lower than those of WT ON GCs (Fig. 6*Ci*; 17.8 ± 0.7 spikes/s; $n = 289$; $p = 0.005$ and $p = 0.01$, respectively). The difference in both peak and maintained firing rates are evident for both $Glra2^{-/-}$ and $Glra3^{-/-}$ GCs across spot diameters smaller than the RF center, however only the maintained rates are significantly lower (Fig. 6*Cii*; $p < 0.01$). These results suggest that the input of both GlyRα2 and GlyRα3 subunits augments the total excitatory response in WT ON GCs.

The peak amplitude (30.0 ± 2.3 spikes/s; $n = 47$) and maintained firing rates (7.0 ± 1.0 spikes/s; $n = 34$) of $Glra2/3^{-/-}$ ON GCs were significantly lower than those of either single KO (Fig. 6*Bi*,*Ci*; $p < 0.001$). This result indicates that GlyRα2 and GlyRα3 subunit inputs contribute separately to the RF center excitatory response of WT ON GCs. They also indicate that the two subunit inputs cooperate to enhance both RF center excitation and the sustained nature of ON GC response (see Fig. 10*A*,*C*).
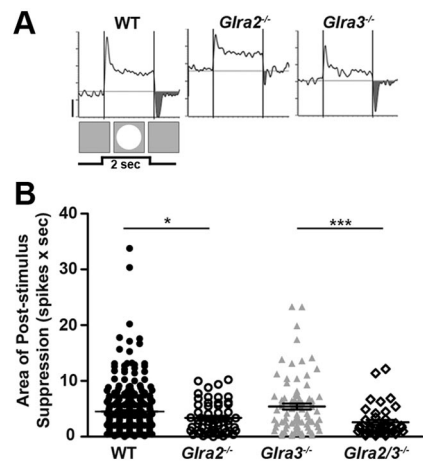

Figure 7. Only GlyRα2-mediated inhibition modulates poststimulus suppression in ON GCs. *A*, Representative PSTH responses of WT and single- and double KO ON GCs during RF center stimulation with a bright (100 cd/m^2) spot. The shaded regions represent poststimulus suppression at the offset of the stimulus (background, 20 cd/m^2). *B*, A scatter plot shows the distribution of the area of poststimulus suppression (spikes × sec) across genotype, which is significantly lower in $Glra2^{-/-}$ (open circles; $n = 57$) compared to WT (closed circles; $n = 284$) but similar in $Glra3^{-/-}$ ON GCs (gray triangles; $n = 84$). The area of poststimulus suppression did not differ between and $Glra2/3^{-/-}$ (open diamonds; $n = 41$) and $Glra2^{-/-}$ ON GCs, but was significantly lower compared to $Glra3^{-/-}$ ON GCs. Scale bar, 20 spikes per second. *$p < 0.05$; ***$p < 0.001$.

WT ON GC response suppression at stimulus offset is specific to GlyRα2 inputs
Like most mammalian GCs, the spiking activity of WT mouse ON GCs is suppressed below spontaneous levels at stimulus offset (poststimulus suppression; Fig. 7*A*, left). In our WT sample, ON GCs remain suppressed on average for 0.66 s after stimulus offset. The etiology of this suppression is not completely understood. A feedforward glycinergic input to ON GCs at stimulus offset has been shown to be generated by the Off pathway and hypothesized to use a crossover inhibitory mechanism (Chen et al., 2010).

To test the hypothesis that GlyRα2 and/or GlyRα3 mediate this input, we compared total poststimulus suppression in ON GCs in each single KO to WT. Consistent with a mechanism mediated by GlyRα2, $Glra2^{-/-}$ ON GCs show less poststimulus suppression compared to WT ON GCs (Fig. 7*B*; 3.4 ± 0.4 spikes × sec, $n = 57$ vs 4.5 ± 0.3 spikes × sec, $n = 284$; $p = 0.01$). Poststimulus suppression in $Glra3^{-/-}$ ON GCs was similar to that in WT (Fig. 7*B*; 5.4 ± 0.5 spikes × sec; $n = 84$; $p = 0.13$). Poststimulus suppression in double KO ON GCs was similar to that in $Glra2^{-/-}$ ON GCs (Fig. 7*B*; 2.6 ± 0.4 spikes × sec; $n = 41$; $p = 0.17$) and significantly lower than that in $Glra3^{-/-}$ ON GCs ($p < 0.001$). These changes most likely do not result from differences in SA levels. Although the SA of GlyRα3 ON GCs is lower compared to that of WT, their poststimulus suppression is similar to that of WT. In contrast, the SA of GlyRα2 ON GCs is similar to that of WT, whereas their poststimulus suppression is significantly less compared to WT.

In summary, both the RF center excitatory response at stimulus onset and response suppression at stimulus offset are lower in $Glra2^{-/-}$ ON GCs compared to WT. In $Glra3^{-/-}$ ON GCs, only the RF center excitatory response is lower. Combined with our results for double KO ON GCs, which show an even greater change in RF excitation than either single KO, suggest that GlyRα2 and GlyRα3 inputs work independently in the On pathway, albeit to the same purpose, to enhance and extend RF center excitation.
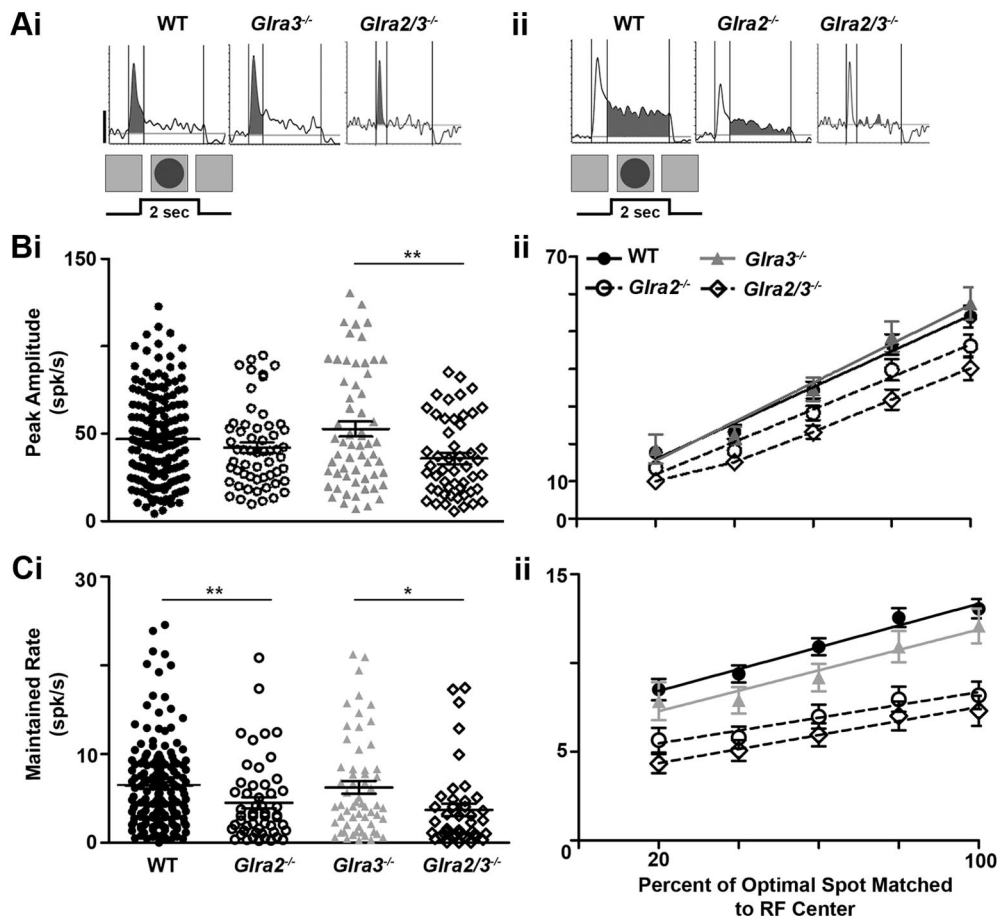
Figure 8. Only GlyRα2-mediated inhibition modulates the receptive field center responses of OFF GCs. *Ai, Aii*, Representative PSTH responses of WT and single- and double KO OFF GCs during RF center stimulation with a dark (3 cd/m^2) spot, whose duration profile is indicated below the stimulus. The shaded regions represent the transient (0–0.4 s) and maintained (0.4–2 s) components of the excitatory response. *Bi*, The scatter plot shows the distribution of peak amplitude responses across genotype and the differences across genotype. The peak amplitudes of both Glra2$^{-/-}$ (open circles; $n = 57$) and Glra3$^{-/-}$ (gray triangles; $n = 61$) are similar compared to WT (closed circles; $n = 174$); that of Glra2/3$^{-/-}$ OFF GCs (open diamonds; $n = 51$) is lower compared to Glra3$^{-/-}$ but similar compared to Glra2$^{-/-}$ OFF GCs. *Bii*, The mean ARFs for each genotype. RF diameter is normalized so that the optimal diameter is plotted at 100%. The slope represents the rate of change in peak amplitude during RF center summation and is similar between WT and single KOs ($p = 0.35$) and single and double KOs ($p = 0.08$). All curves were analyzed using a linear regression and the goodness of fit for all genotypes; $R^2 = 0.98$. *Ci*, The scatter plot shows the distribution of maintained firing rate across genotype and the differences across genotype. The maintained firing rates are lower in Glra2$^{-/-}$ OFF GCs (open circles; $n = 52$) compared to WT (closed circles; $n = 167$) but similar in Glra3$^{-/-}$ OFF GCs (gray triangles; $n = 59$) compared to WT. The maintained firing rate also in Glra2/3$^{-/-}$ (open diamonds; $n = 42$) is lower than that in Glra3$^{-/-}$ OFF GCs but similar compared to Glra2$^{-/-}$ OFF GCs. *Cii*, The mean ARFs for each genotype. RF diameter is normalized so that the optimal diameter is plotted at 100%. The slope represents the rate of change in the maintained firing rate during RF center summation. The slope differs between Glra2$^{-/-}$ and WT OFF GCs ($p = 0.01$) but is similar between Glra3$^{-/-}$ and WT ($p = 0.71$) OFF GCs. The slopes did not differ between single- and double KOs OFF GCs ($p = 0.07$). All curves were analyzed using a linear regression and the goodness of fit for all genotypes; $R^2 = 0.95$. Scale bar, 20 spikes per second. *$p < 0.05$; **$p < 0.01$.

WT OFF GC temporal responses are modulated by GlyRα2 input

The onset of a dark spot of standing contrast whose dimensions are within or match the RF center evokes an excitatory response in WT OFF GCs. Like their WT ON counterparts, WT OFF GCs show an initial transient peak within 0.40 s of stimulus onset (Fig. 8 *Ai*, left). In 77% of WT OFF GCs (134 of 174), this is followed by a maintained excitation that is temporally matched to the stimulus (Fig. 3*Bi*), whereas in the other 23%, the excitatory response declines to SA level before stimulus offset (Fig. 3*Ci*). Previous publications also have described two functional types of WT OFF mouse GCs (Pang et al., 2003; Murphy and Rieke, 2006; van Wyk et al., 2009), although the stimulus durations they used were significantly shorter than 2 s. Although the morphological identity of the GCs sampled in our extracellular optic nerve recordings are not known, we assume that they are A-type for the following reasons: Our optic nerve recordings target GCs with the largest axons (Boycott and Wässle, 1974). Optic nerve recordings only sample responses of ON- and OFF-center GCs.

Table 2. Proportion of OFF GCs with sustained or transient responses across genotype

	Sustained (%)	Transient (%)	Total OFF GCs
WT	77 ($n = 134$)	23 ($n = 40$)	174
Glra2$^{-/-}$*	60 ($n = 34$)	40 ($n = 23$)	57
Glra3$^{-/-}$	75 ($n = 46$)	25 ($n = 15$)	61
Glra2/3$^{-/-}$*	45 ($n = 23$)	55 ($n = 28$)	51

The proportions of OFF sustained and OFF transient GCs are given for each genotype. The proportions of OFF sustained and OFF transient GCs are similar between WT and Glra3$^{-/-}$. In contrast, Glra2$^{-/-}$ and Glra2/3$^{-/-}$ OFF GCs have more transient than sustained GCs compared to WT.

*$p < 0.05$.

The GCs recorded have brisk visually evoked responses and linear RF center summation (Kuffler, 1953; Enroth-Cugell and Robson, 1966).

Across Glra2$^{-/-}$, Glra3$^{-/-}$, and Glra2/3$^{-/-}$ OFF GCs, we found both sustained and transient GCs (Fig. 3*Aii–Civ*), and their proportions in Glra3$^{-/-}$ OFF GCs were similar to those of WT (Table 2). In contrast, Glra2$^{-/-}$ and Glra2/3$^{-/-}$ OFF GCs had

more transient than sustained responses compared to WT (Table 2; $Glra2^{-/-}$, $p = 0.01$; $Glra2/3^{-/-}$, $p \leq 0.001$; χ^2). As a consequence, we did not use a sustained/transient criterion to group OFF GCs. Instead, we compared all OFF GCs in KO mice to WT to define general trends in the contribution of GlyRα2 and GlyRα3 inhibition.

WT OFF GC receptive field center excitation is modulated by GlyRα2 input

The transient peak response of $Glra3^{-/-}$ and WT OFF GC RF center responses at the optimal spot diameter were similar (Fig. 8 *Ai,Bi*; 52.7 ± 4.3 spikes/s, $n = 61$ vs 47.0 ± 2.0 spikes/s, $n = 174$; $p = 0.22$), as were their maintained firing rates (Fig. 8 *Ai,Ci*; 6.2 ± 0.7 spikes/s, $n = 59$ vs 6.5 ± 0.4 spikes/s, $n = 167$; $p = 0.80$). These similarities were maintained across all spot diameters within the RF center (Fig. 8 *Bii,Cii*; $p > 0.05$ for both). No other differences were noted in any aspect of the RF center response at stimulus onset or offset, leading to the conclusion that GlyRα3 input does not modulate OFF GC RF center responses.

The transient peak response of $Glra2^{-/-}$ OFF GCs at all spot diameters within the RF center was similar to that of WT (Fig. 8 *Bi,Bii*; optimal, 42.0 ± 3.0 spikes/s; $n = 57$; $p = 0.20$; all diameters, $p > 0.05$). The maintained firing rates of $Glra2^{-/-}$ OFF GC RF center excitatory responses were significantly lower than those of WT OFF GCs both at the optimal diameter (Fig. 8 *Aii,Ci*; 4.5 ± 0.6 spikes/s, $n = 52$ vs 6.5 ± 0.4 spikes/s, $n = 167$; $p = 0.009$) and across all spot diameters within the RF center (Fig. 8 *Cii*; $p < 0.001$). The difference in the maintained response component causes the increase in transient GlyRα2 OFF GCs compared to WT described above.

Both the peak RF center response of double KO OFF GCs (Fig. 8 *Ai,Bi*; peak, 36.0 ± 3.1 spikes/s; $n = 51$; $p = 0.17$) and the maintained response were similar to those of $Glra2^{-/-}$ OFF GCs (Fig. 8 *Ci*; maintained, 3.7 ± 0.7 spikes/s; $n = 42$; $p = 0.40$). Consequently, they were significantly lower compared to $Glra3^{-/-}$ OFF GCs ($p = 0.002$ and $p = 0.02$, respectively).

OFF GCs also exhibit response suppression at stimulus offset (Fig. 9A). $Glra2^{-/-}$ OFF GCs had significantly less poststimulus suppression compared to WT (Fig. 9B; 0.8 ± 0.1 spikes × sec, $n = 56$ vs 1.7 ± 0.1 spikes × sec, $n = 168$; $p < 0.001$). Poststimulus suppression in $Glra3^{-/-}$ OFF GCs was similar to that in WT OFF GCs (Fig. 9B; 2.2 ± 0.3 spikes × sec; $n = 59$; $p = 0.06$). Poststimulus suppression in double KO OFF GCs (1.1 ± 0.2 spikes × sec; $n = 50$) was similar to that in $Glra2^{-/-}$ OFF GCs ($p = 0.10$) and, as a consequence, lower than in $Glra3^{-/-}$ OFF GCs ($p = 0.001$).

Our results demonstrate a novel role for GlyRα2-mediated inhibition in modulating the RF center response of WT OFF GCs and relative to GlyRα3-mediated inhibition, the only one that modulates WT OFF GC responses. The exact role of GlyRα1 input, which is the predominant glycinergic synaptic input to mouse rod and cone Off bipolar cells as well as A-type GCs (Majumdar et al., 2007) remains to be defined and will require conditional elimination of its expression. The differences that we observed for GlyRα2 in ON GCs, namely, less excitation and less suppression, are the same as those we observe in OFF GCs. This indicates that GlyRα2 uses a similar inhibitory mechanism in both pathways to the same end, to enhance the excitatory RF center response and match it to stimulus duration.
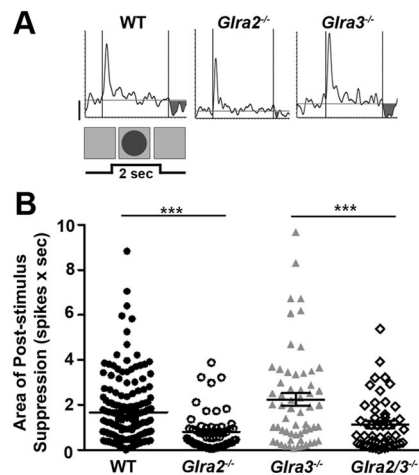

Figure 9. Only GlyRα2-mediated inhibition modulates poststimulus suppression in OFF GCs. *A*, Representative PSTH responses of WT and single KO OFF GCs during receptive field center stimulation with a dark (3 cd/m^2) spot. The shaded regions represent poststimulus suppression at the offset of the stimulus (background, 20 cd/m^2). *B*, A scatter plot shows the distribution of the area of poststimulus suppression (spikes × sec) across genotype, which is lower in $Glra2^{-/-}$ (open circles; $n = 56$) compared to WT OFF GCs (closed circles; $n = 168$) but similar in $Glra3^{-/-}$ OFF GCs (gray triangles; $n = 59$). The area of poststimulus suppression in $Glra2/3^{-/-}$ OFF GCs (open diamonds; $n = 50$) is lower than in $Glra3^{-/-}$ OFF GCs but similar to that in $Glra2^{-/-}$ OFF GCs. Scale bar, 20 spikes per second. ***$p < 0.001$.

Discussion

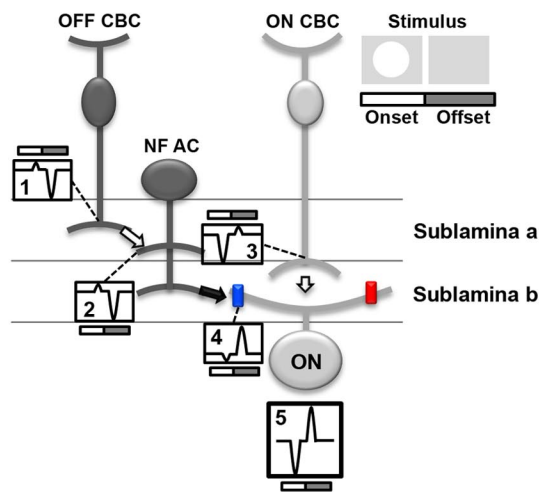### GlyRα2 and GlyRα3 subunit-specific modulation of ON and OFF GC RF center temporal responses

Our results show GlyRα2 subunit-specific control over the maintained component of the RF center response of OFF GCs to stimulus onset and poststimulus suppression. In this pathway, GlyRα2 functions to enhance GC RF center excitation and temporally match the excitatory response to stimulus duration. In ON GCs, temporal response components are governed by both GlyRα2 and GlyRα3 subunit inputs, which appear to contribute separately but function together to perform the same response enhancement and temporal matching. We found no evidence of either subunit input alone mediating spatial aspects of the RF response, which is consistent with an established role of glycinergic inhibition in the modulation of temporal and not spatial properties of the GC visual response (Bolz et al., 1985; Stone and Pinto, 1992; O'Brien et al., 2003; Chen et al., 2010).

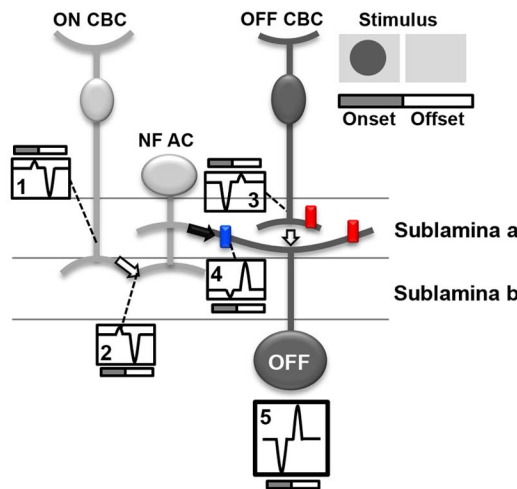### GlyRα2 and GlyRα3 subunits modulate inhibition slower than receptor kinetics

In $Glra2^{-/-}$ OFF GCs, a lower maintained excitatory response compared to WT results in more transient responses both in $Glra2^{-/-}$ and $Glra2/3^{-/-}$ double KO mice. Spontaneous GlyRα1 and GlyRα3 IPSCs (Ivanova et al., 2006; Majumdar et al., 2007; Weiss et al., 2008) and light-evoked glycinergic IPSCs (Pang et al., 2007; Manookin et al., 2008) have been shown in cellular components of the Off pathway. Thus, our results define a new role for GlyRα2 inhibition in shaping the response of WT OFF GCs to match stimulus duration.

GlyRα2 and GlyRα3 control of the maintained response is slow (between 0.4 and 2 s) compared to their receptor kinetics (mean decay τ, GlyRα2, ~27 ms; GlyRα3, ~11ms) (Weiss et al., 2008). This difference is most easily explained by a prolonged or asynchronous release of presynaptic neurotransmitter that shapes the inhibitory input controlling the maintained response, similar to the timing of inhibitory inputs that shape BC light-
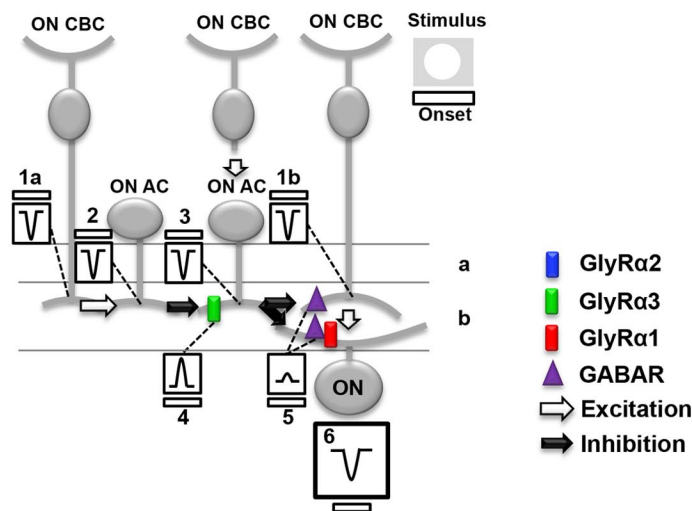
A GlyRα2 Crossover Inhibition Off to On pathway

B GlyRα2 Crossover Inhibition On to Off pathway

C GlyRα3 Serial Inhibition in the On pathway

Figure 10. GlyRα2 and GlyRα3 mediate inhibition using different inhibitory circuits. *A–C*, Schematic diagrams of the proposed roles of GlyRα2 and GlyRα3 in the WT mouse On and Off retinal pathways are shown. Each diagram illustrates a basic retina circuit that is consistent with the results presented. The diagrams in the top right corners illustrate the stimulus and the timing of its onset and offset. Within each circuit, the numbered boxes represent the current evoked at stimulus onset and offset. Nota bene: Currents are represented with transient time course for simplicity. The currents in the boxes do not reflect the temporal properties of the

evoked inhibition (Tachibana, 1999; Eggers and Lukasiewicz, 2006; Eggers et al., 2007).

GlyRα2 and GlyRα3 enhance ON and OFF GC RF center excitation through separate inhibitory mechanisms

GlyRα2 mediates crossover inhibition in both the On and Off pathways

The absence of GlyRα2 expression creates the same changes in ON and OFF GC RF center responses. Both the transient and sustained components of the RF center excitatory responses at stimulus onset and poststimulus suppression are significantly lower than those of WT. Less excitation is inconsistent with the removal of direct inhibition. Removal of serial inhibitory input will result in less excitation at stimulus onset; however poststimulus suppression, arising from inhibitory inputs in the opposite pathway, should be unchanged. The most parsimonious explanation for our result is that GlyRα2 mediates crossover inhibition from the Off to the On as well as the On to Off WT pathways. Glycinergic crossover inhibition has

←

currents, as described in Results. *A*, GlyRα2 mediates crossover inhibition from the Off to the On pathway. At stimulus onset (white bar), the NF AC is driven by an OFF CBC (Box 1), which produces a small outward current (Box 2). The NF AC, using a crossover inhibitory mechanism, inverts the polarity of the current via GlyRα2 (blue), producing a current in the ON GC (Box 4) that enhances the current from its presynaptic ON CBC (Box 3). At stimulus offset (gray bar), a similar mechanism transfers an inverted polarity current from the Off to the On pathway, which enhances poststimulus suppression. The spiking response of the GC is governed by the summation of the inputs (Box 5). *B*, GlyRα2 mediates crossover inhibition from the On to the Off pathway. Similar to the description in *A*, at stimulus onset (gray bar), the NF AC is driven by an ON CBC (Box 1), which produces a small outward current (Box 2). The NF AC, using a crossover inhibitory mechanism inverts the polarity of the current via GlyRα2 (blue), producing a current in the OFF GC (Box 4) that enhances the current from its presynaptic OFF CBC (Box 3). At stimulus offset (white bar), a similar mechanism transfers an inverted polarity current from the Off to the On pathway, which enhances poststimulus suppression. The spiking response of the GC is governed by the summation of the inputs (Box 5). *C*, GlyRα3 mediates serial inhibition in the On pathway. At stimulus onset (white bar), ON CBCs depolarize (Boxes 1a and 1b represent currents in all CBCs). The ON CBC (far left) targets an ON AC producing an inward current (Box 2). Using GlyRα3 (green), this distal ON AC produces an outward current in the proximal ON AC (Box 4), which is summed with the inward current produced via input from its presynaptic ON CBC (Box 3). The proximal ON AC targets either the ON CBC (far right) at a GABA receptor (purple) or an ON GC at either a GABA receptor (purple) or a GlyRα1R (red). Because the proximal ON AC output is controlled by its ON AC inhibitory input, the outward current (Box 5) is small. Depending on the postsynaptic target of the proximal ON AC, the GCs total current (Box 6) reflects either the input from its presynaptic CBC (Box 1b) or from the inputs from its presynaptic CBC and ON AC (Box 5).

been shown to augment both excitation at stimulus onset and suppression at stimulus offset in rabbit GCs (Roska and Werblin, 2001; Roska et al., 2006; Molnar and Werblin, 2007; Hsueh et al., 2008; Molnar et al., 2009; Chen et al., 2010). In addition, mouse OFF GCs receive glycinergic inhibitory inputs from the On pathway (van Wyk et al., 2009).

Figure 10A illustrates a circuit in which GlyRα2 mediates crossover input from the Off to On pathway. The GlyRα2 receptor is positioned as the target of a narrow field (NF) AC, where it mediates inhibition to an ON GC. We have eliminated ON cone BCs (CBCs) as the target because they lack spontaneous and evoked glycinergic IPSCs (Ivanova et al., 2006; Eggers et al., 2007). At the onset of a bright-spot stimulus (currents under white portion of stimulus profile bars), the primary inward current that governs excitation in ON GCs (Fig. 10A, Box 5) arises from ON CBCs (Box 3). In the Off pathway, stimulus onset produces a small outward current in OFF CBCs (Box 1) that provides input and produces a response in the NF AC (Box 2). Crossover inhibition inverts this current, and the NF AC synaptic input produces a current in the ON GC (Box 4) with the same sign as its ON CBC input (Box 3). In WT ON GCs, this mechanism enhances excitation, and in the absence of GlyRα2 input, only the ON CBC input drives the ON GC response, and the stimulus evokes less excitation. The offset of the bright spot (currents under the gray portion of the stimulus profile bars) eliminates the excitatory input from the ON CBC and induces a small outward current (Box 3). At the same time, OFF CBC excitation elicits a large inward current in the NF AC (Box 2). Crossover inhibition inverts current polarity and the NF AC input produces a current in the ON GC (Box 4) of the same sign as its ON CBC input (Box 3). This enhances response suppression in WT ON GCs (Box 5), and the absence of GlyRα2 input reduces suppression.

Changes in RF center responses of OFF GCs in the absence of GlyRα2 are the same as those in ON GCs, which suggests a similar GlyRα2 inhibitory mechanism in the On and Off pathways (Fig. 10B). Although the receptor subunit was unknown at the time, On-to-Off pathway inhibition was predicted to occur via an intermediate glycinergic AC in cat GCs (Wässle et al., 1986). Given its localization throughout the IPL (Heinze et al., 2007), our results suggest that GlyRα2 is a subunit that mediates inhibitory inputs from the On to the Off pathway and vice versa.

Figure 10B illustrates GlyRα2-mediated crossover input from the On to the Off pathway. Here the GlyRα2 receptor is the target of a NF AC for two reasons. All spontaneous and glycine evoked IPSCs in OFF CBCs are mediated by GlyRα1 (Ivanova et al., 2006). Glycinergic IPSCs with slower kinetics remain in A2 OFF GCs in the absence of their dominant GlyRα1 synaptic input (Majumdar et al., 2007). The onset of a dark spot initiates excitation in OFF CBCs (currents under gray portion of stimulus profile bars). Using a NF AC, the same crossover inhibitory mechanisms described for the Off to the On pathway (Fig. 10A) enhance the RF excitatory response as well as response suppression in WT OFF GCs. Again, the absence of GlyRα2 input lowers response excitation and suppression. It should be noted that concatenated circuits have been observed previously (Anderson et al., 2011). If they provide input to the NF AC that mediates crossover inhibition, then the position of the GlyRα2 receptor could differ from our placement in Figure 10, A and B. What is not in question is that our observations are consistent with a role of the GlyRα2 receptor and a crossover inhibitory circuit that contributes to GC RF center response enhancement.

GlyRα3 mediates serial inhibition in the On pathway

Both RF center transient and maintained response components of $Glra3^{-/-}$ ON GCs are lower than those of WT. The absence of GlyRα3 inhibition does not affect poststimulus suppression, and we therefore predict that GlyRα3 uses a different mechanism, serial inhibition, in the On pathway. GABAergic feedback to the RF center of rabbit local edge detector GCs is controlled by serial glycinergic inhibition (Russell and Werblin, 2010), and this mechanism also governs salamander GC responses (Zhang et al., 1997).

Figure 10C illustrates GlyRα3-mediated serial inhibitory input within the On pathway. This pathway is shown separately for clarity, although GlyRα2 and GlyRα3 could work together in the same circuit. The GlyRα3 receptor is located on the ON AC most proximal to the ON GC, as the target of a distal ON AC. All AC processes are confined to the On sublaminae because $Glra3^{-/-}$ OFF GC RF responses are similar to those of WT. ON CBCs only show GABAergic sIPSCs; therefore, if they are the target, then the proximal ON AC is GABAergic (Eggers et al., 2007), whereas if the target is an ON GC, the proximal ON AC can be glycinergic targeting GlyRα1Rs (Ivanova et al., 2006) or GABAergic targeting GABA$_A$Rs (Eggers et al., 2007). At the onset of a bright-spot stimulus (Fig. 10C, currents under white stimulus profile bars), an excitatory response arises in ON CBCs (Boxes 1a, 1b), resulting in inward currents in ON ACs (Boxes 2, 3). GlyRα3-mediated inhibition from the distal ON AC (Box 4) reduces the inward current in the proximal ON AC (Box 5). This reduces its inhibitory output to the postsynaptic target (WT ON CBC or GC). The absence of GlyRα3 expression eliminates the inhibitory input to the proximal AC and increases its inhibitory input. When its target is the ON CBC, this reduces excitatory input to the ON GC. When its target is the ON GC, excitation decreases because direct inhibition increases. Regardless, the absence of GlyRα3 expression reduces stimulus evoked spiking in the ON GC (Box 6).

Summary

Our findings extend the previous literature that demonstrated a significant role of glycinergic inhibition in shaping visual responses in the retina. Our results define novel roles of two glycine subunits not only in their selectivity within the On and Off pathways, but also in the specific inhibitory mechanisms that they employ to modulate GC visual function. One question arises whenever the role of ACs in retinal function is discussed: Why are there so many diverse AC classes? In light of this question, our results could be interpreted as evidence to support the idea that multiple ACs are required to target each subunit-specific input within the retinal parallel pathways and that different ACs are required to modulate both the transient and sustained aspects of the visual response.

References

Anderson JR, Jones BW, Watt CB, Shaw MV, Yang JH, Demill D, Lauritzen JS, Lin Y, Rapp KD, Mastronarde D, Koshevoy P, Grimm B, Tasdizen T, Whitaker R, Marc RE (2011) Exploring the retinal connectome. Mol Vis 17:355–379.

Barthel LK, Raymond PA (1990) Improved method for obtaining 3-microns cryosections for immunocytochemistry. J Histochem Cytochem 38:1383–1388.

Bolz J, Thier P, Voigt T, Wässle H (1985) Action and localization of glycine and taurine in the cat retina. J Physiol 362:395–413.

Bormann J (2000) The "ABC" of GABA receptors. Trends Pharmacol Sci 21:16–19.

Boycott BB, Wässle H (1974) The morphological types of ganglion cells of the domestic cat's retina. J Physiol 240:397–419.

Caldwell JH, Daw NW (1978) Effects of picrotoxin and strychnine on rabbit

retinal ganglion cells: changes in centre surround receptive fields. J Physiol 276:299–310.

Chen X, Hsueh HA, Greenberg K, Werblin FS (2010) Three forms of spatial temporal feedforward inhibition are common to different ganglion cell types in rabbit retina. J Neurophysiol 103:2618–2632.

Chen X, Hsueh HA, Werblin FS (2011) Amacrine-to-amacrine cell inhibition: Spatiotemporal properties of GABA and glycine pathways. Vis Neurosci 28:193–204.

Cook PB, McReynolds JS (1998) Modulation of sustained and transient lateral inhibitory mechanisms in the mudpuppy retina during light adaptation. J Neurophysiol 79:197–204.

Cui J, Ma Y-P, Lipton SA, Pan Z-H (2003) Glycine receptors and glycinergic synaptic input at the axon terminals of mammalian retinal rod bipolar cells. J Physiol 533 3:895–909.

Eggers ED, Lukasiewicz PD (2006) Receptor and transmitter release properties set the time course of retinal inhibition. J Neurosci 26:9413–9425.

Eggers ED, Lukasiewicz PD (2010) Interneuron circuits tune inhibition in retinal bipolar cells. J Neurophysiol 103:25–37.

Eggers ED, Lukasiewicz PD (2011) Multiple pathways of inhibition shape bipolar cell responses in the retina. Vis Neurosci 28:95–108.

Eggers ED, McCall MA, Lukasiewicz PD (2007) Presynaptic inhibition differentially shapes transmission in distinct circuits in the mouse retina. J Physiol 582:569–582.

Enroth-Cugell C, Robson JG (1966) The contrast sensitivity of retinal ganglion cells of the cat. J Physiol 187:517–552.

Enz R, Bormann J (1995) Expression of glycine receptor subunits and gephyrin in single bipolar cells of the rat retina. Vis Neurosci 12:507–517.

Flores-Herr N, Protti DA, Wässle H (2001) Synaptic currents generating the inhibitory surround of ganglion cells in the mammalian retina. J Neurosci 21:4852–4863.

Gregg RG, Kamermans M, Klooster J, Lukasiewicz PD, Peachey NS, Vessey KA, McCall MA (2007) Nyctalopin expression in retinal bipolar cells restores visual function in a mouse model of complete X-linked congenital stationary night blindness. J Neurophysiol 98:3023–3033.

Grimes WN, Zhang J, Graydon CW, Kachar B, Diamond JS (2010) Retinal parallel processors: more than 100 independent microcircuits operate within a single interneuron. Neuron 65:873–885.

Grudzinska J, Schemm R, Haeger S, Nicke A, Schmalzing G, Betz H, Laube B (2005) The beta subunit determines the ligand binding properties of synaptic glycine receptors. Neuron 45:727–739.

Harvey RJ, Depner UB, Wässle H, Ahmadi S, Heindl C, Reinold H, Smart TG, Harvey K, Schütz B, Abo-Salem OM, Zimmer A, Poisbeau P, Welzl H, Wolfer DP, Betz H, Zeilhofer HU, Müller U (2004) GlyR alpha3: an essential target for spinal PGE2-mediated inflammatory pain sensitization. Science 304:884–887.

Haverkamp S, Müller U, Harvey K, Harvey RJ, Betz H, Wässle H (2003) Diversity of glycine receptors in the mouse retina: localization of the alpha3 subunit. J Comp Neurol 465:524–539.

Heinze L, Harvey RJ, Haverkamp S, Wässle H (2007) Diversity of glycine receptors in the mouse retina: localization of the alpha4 subunit. J Comp Neurol 500:693–707.

Hsueh HA, Molnar A, Werblin FS (2008) Amacrine-to-amacrine cell inhibition in the rabbit retina. J Neurophysiol 100:2077–2088.

Ivanova E, Müller U, Wässle H (2006) Characterization of the glycinergic input to bipolar cells of the mouse retina. Eur J Neurosci 23:350–364.

Kuffler SW (1953) Discharge patterns and functional organization of mammalian retina. J Neurophysiol 16:37–68.

MacNeil MA, Masland RH (1998) Extreme diversity among amacrine cells: implications for function. Neuron 20:971–982.

MacNeil MA, Heussy JK, Dacheux RF, Raviola E, Masland RH (1999) The shapes and numbers of amacrine cells: matching of photofilled with Golgi-stained cells in the rabbit retina and comparison with other mammalian species. J Comp Neurol 413:305–326.

Majumdar S, Heinze L, Haverkamp S, Ivanova E, Wässle H (2007) Glycine receptors of A-type ganglion cells of the mouse retina. Vis Neurosci 24:471–487.

Manookin MB, Beaudoin DL, Ernst ZR, Flagel LJ, Demb JB (2008) Disinhibition combines with excitation to extend the operating range of the OFF visual pathway in daylight. J Neurosci 28:4136–4150.

Menger N, Pow DV, Wässle H (1998) Glycinergic amacrine cells of the rat retina. J Comp Neurol 401:34–46.

Molnar A, Werblin F (2007) Inhibitory feedback shapes bipolar cell responses in the rabbit retina. J Neurophysiol 98:3423–3435.

Molnar A, Hsueh HA, Roska B, Werblin FS (2009) Crossover inhibition in the retina: circuitry that compensates for nonlinear rectifying synaptic transmission. J Comput Neurosci 27:569–590.

Murphy GJ, Rieke F (2006) Network variability limits stimulus-evoked spike timing precision in retinal ganglion cells. Neuron 52:511–524.

O'Brien BJ, Richardson RC, Berson DM (2003) Inhibitory network properties shaping the light evoked responses of cat alpha retinal ganglion cells. Vis Neurosci 20:351–361.

Pang JJ, Gao F, Wu SM (2003) Light-evoked excitatory and inhibitory synaptic inputs to ON and OFF alpha ganglion cells in the mouse retina. J Neurosci 23:6063–6073.

Pang JJ, Abd-El-Barr MM, Gao F, Bramblett DE, Paul DL, Wu SM (2007) Relative contributions of rod and cone bipolar cell inputs to AII amacrine cell light responses in the mouse retina. J Physiol 580:397–410.

Roska B, Werblin F (2001) Vertical interactions across ten parallel, stacked representations in the mammalian retina. Nature 410:583–587.

Roska B, Nemeth E, Orzo L, Werblin FS (2000) Three levels of lateral inhibition: a space-time study of the retina of the tiger salamander. J Neurosci 20:1941–1951.

Roska B, Molnar A, Werblin FS (2006) Parallel processing in retinal ganglion cells: how integration of space-time patterns of excitation and inhibition form the spiking output. J Neurophysiol 95:3810–3822.

Russell TL, Werblin FS (2010) Retinal synaptic pathways underlying the response of the rabbit local edge detector. J Neurophysiol 103:2757–2769.

Sagdullaev BT, McCall MA (2005) Stimulus size and intensity alter fundamental receptive-field properties of mouse retinal ganglion cells *in vivo*. Vis Neurosci 22:649–659.

Sagdullaev BT, DeMarco PJ, McCall MA (2004) Improved contact lens electrode for corneal ERG recordings in mice. Doc Ophthalmol 108:181–184.

Sassoè-Pognetto M, Wässle H, Grünert U (1994) Glycinergic synapses in the rod pathway of the rat retina: cone bipolar cells express the α1 subunit of the glycine receptor. J Neurosci 14:5131–5146.

Stone C, Pinto LH (1992) Receptive field organization of retinal ganglion cells in the spastic mutant mouse. J Physiol 456:125–142.

Tachibana M (1999) Regulation of transmitter release from retinal bipolar cells Prog Biophys Mol Biol 72:109–133.

van Wyk M, Wässle H, Taylor WR (2009) Receptive field properties of ON- and OFF-ganglion cells in the mouse retina. Vis Neurosci 26:297–308.

Wässle H, Schäfer-Trenkler I, Voigt, T (1986) Analysis of a glycinergic inhibitory pathway in the cat retina. J Neurosci 6:594–604.

Wässle H, Heinze L, Ivanova E, Majumdar S, Weiss J, Harvey RJ, Haverkamp S (2009) Glycinergic transmission in the mammalian retina. Front Mol Neurosci 2:1–12.

Webb TI, Lynch JW (2007) Molecular pharmacology of the glycine receptor chloride channel. Curr Pharm Des 13:2350–2367.

Weiss J, O'Sullivan GA, Heinze L, Chen HX, Betz H, Wässle H (2008) Glycinergic input of small-field amacrine cells in the retinas of wildtype and glycine receptor deficient mice. Mol Cell Neurosci 37:40–55.

Young-Pearse TL, Ivic L, Kriegstein AR, Cepko CL (2006) Characterization of mice with targeted deletion of glycine receptor alpha 2. Mol Cell Biol 26:5728–5734.

Zhang J, Jung CS, Slaughter MM (1997) Serial inhibitory synapses in retina. Vis Neurosci 14:553–563.